Computers and Chemical Engineering 183 (2024) 108621

Contents lists available at ScienceDirect

Computers and Chemical Engineering

journal homepage: www.elsevier.com/locate/cace

Hierarchical heat transfer modeling of a continuous millireactor

Moritz J. Begall [a], Frank Herbstritt [b], Anne-Laura Sengen [b], Adel Mhamdi [a], Joachim Heck [b], Alexander Mitsos [a,c,*]

[a] RWTH Aachen University, Aachener Verfahrenstechnik - Process Systems Engineering (AVT.SVT), Forckenbeckstraße 51, 52074, Aachen, Germany
[b] Ehrfeld Mikrotechnik GmbH, Mikroforum Ring 1, 55234, Wendelsheim, Germany
[c] Forschungszentrum Jülich GmbH, Institute of Energy & Climate Research (IEK-10), Wilhelm-Johnen-Straße, 52428, Jülich, Germany

ARTICLE INFO

Keywords:
Millireactor
CFD
Hydrodynamics
Heat transfer

ABSTRACT

Continuous millireactors are important but complex devices. Knowledge of their heat transfer characteristics is essential for their design and operation, but can be difficult to determine with experiments alone. We present a hierarchical CFD model which simulates the fluid flow and heat transfer of a Miprowa Lab millireactor in three increasing levels of detail, and which is validated with experimental data. The model is then used to infer additional process information that is not available via physical measurements and which in turn is used to calculate heat transfer coefficients of the channel. The computational results show that using only the experimental values under-predicts the heat transfer coefficients with a mismatch of up to 11 %. Quantifying this deviation is a valuable benefit provided by the model. The model paves the way for predicting the heat transfer behavior of the reactor for different process conditions or even model-based optimization of the reactor geometry.

1. Introduction

Continuous flow processing is an established production method for bulk chemicals, and is increasingly being used for small-scale processes and specialty chemicals (Gürsel et al., 2012). While these areas still rely in a large part on batch processing (Calabrese and Pissavini, 2011), continuous flow processing in millireactors comes with a variety of advantages. These include a higher yield, selectivity and energy efficiency (Calabrese and Pissavini, 2011), enabled by the tight control of process parameters (Roberge et al., 2014). The latter is especially important for fast, highly exothermic reactions, which require fast heat removal. The high surface to volume ratio of millireactors makes them especially suitable for these applications (Sengen et al., 2017). Additionally, their small holdup, together with their good controllability, can provide safety benefits when working with dangerous substances (Jensen, 2017). However, as these devices can be very complex, often containing internal mixing elements with intricate geometries, they can be difficult to characterize, especially experimentally, as not all properties of interest may be available via measurements.

Computational fluid dynamics (CFD) can help to overcome these challenges, and is widely used to study small-scale devices (Mitsos et al., 2004, 2007; An et al., 2012; Woldemariam et al., 2016; Schönfeld and Hardt, 2004; Shi et al., 2012; Buchelli et al., 2005; Amini et al., 2013; Brahim et al., 2003; Rahimi et al., 2009; Gobert et al., 2017). Since it enables the evaluation at arbitrary points inside the computational domain, it facilitates the extraction of process data and complements and augments experimental characterizations. We have already successfully employed CFD in previous work, using it to manually find geometry modifications of the Miprowa Lab millireactor which reduced its fouling potential (Begall et al., 2018), and coupling it with a Bayesian optimization algorithm to automatically find geometry configurations that reduce areas with stagnating flow and improve the mixing efficiency of the reactor (Begall et al., 2023).

Among the applications of the Miprowa Lab millireactor are polymerization processes, which require precise temperature control to achieve a consistent product quality. Consequently, in this article, we are interested in the heat transfer behavior of this reactor, and want to determine overall heat transfer coefficients for a range of operating conditions. Heat transfer phenomena in millistructured devices are an ongoing research topic, and CFD is increasingly being used for its investigation, e.g., in laminar heat exchangers and reactors (Rodríguez-Guerra et al., 2016) and tubular loop polymerization reactors (Gao et al., 2010). What differentiates the case study investigated in this work is the highly complex geometry of the Miprowa Lab reactor, and the correspondingly complicated flow field which requires a high degree of accuracy and computational resources. We focus on a test

* Corresponding author at: RWTH Aachen University, Aachener Verfahrenstechnik - Process Systems Engineering (AVT.SVT), Forckenbeckstraße 51, 52074, Aachen, Germany.
E-mail address: amitsos@alum.mit.edu (A. Mitsos).

https://doi.org/10.1016/j.compchemeng.2024.108621
Received 5 April 2023; Received in revised form 31 January 2024; Accepted 4 February 2024
Available online 7 February 2024

channel which was specially designed for the experimental characterization of the Miprowa Lab reactor. In a first step, we introduce a hierarchical CFD model, which features three levels of increasing detail to computationally approximate the physical test channel. We then show that CFD simulations can predict the results obtained via experiments with good accuracy. Building on that, we then infer additional information from the CFD model, circumventing the limitations of the experimental setup: The simulations yield the temperatures at any desired point inside the computational domain, including right at the channel wall, while experimentally, only the near-wall temperatures can be measured. It follows that experimental data can only be used to calculate approximate heat transfer coefficients, but it was previously unclear how precise these estimates are. The CFD simulations however allow to compute heat transfer coefficients using both the near-wall and actual wall temperatures, thus making the difference quantifiable. Furthermore, this enables the derivation of correction factors, which then allow the calculation of heat transfer coefficients from experimental measurements with a high degree of accuracy.

2. Methods

2.1. Miprowa test channel

The Miprowa Lab millireactor developed by Ehrfeld Mikrotechnik is a shell and tube heat exchanger type reactor. It contains eight process channels, which are arranged in series and are each 300 mm long. The test channel investigated in this work is however a single channel of only 54 mm length. It was designed specifically to characterize the heat transfer performance of the Miprowa Lab, and thus retains its rectangular shape and interior dimensions of 12 mm by 1.5 mm. Through the flat form of the channel, heat can be transferred more effectively than with a round or square cross section of the same area due to the larger surface to volume ratio. Inside the channel, three layers of steel mixing elements are inserted, forming a three-dimensional grid. The elements have a fin angle of 45°, fin width of 1 mm and fin distance of 2 mm. To facilitate the insertion and removal of the mixing elements, they are slightly thinner than a third of the channel height, thus leaving a gap of nominally 0.075 mm between the elements and channel walls, as well as between the individual elements. A cutaway showing the lower half of the channel is shown in Fig. 1.

The first 18 mm of the test channel are made of PTFE and ensure that the flow of the process fluid is fully developed when it enters the 36 mm long second part of the channel, which consists of an inner copper body and an outer brass body, between which a service fluid flows to heat or cool the channel. The length of the channel was chosen to be long enough for a temperature profile to develop between in- and outlet, but short enough to still be able to measure meaningful exit temperatures of the process fluid even for low flow rates (not thermally equilibrated with the service fluid). Four sensor ports for PT100 temperature sensors are present to measure the inlet and outlet temperatures of the process fluid, as well as the temperatures at two locations inside the copper body. Due to manufacturing limitations, it is not possible to place the sensors directly at the channel walls. The sensors in the copper body are placed 2.45 mm away from the channel walls, and 3.5 mm away from the start and end of the heat transfer section of the channel, respectively. The position of the temperature sensor near the end of the copper body is shown in Fig. 2.

2.2. Experimental setup

The experiments which form the basis of this investigation were conducted at Ehrfeld Mikrotechnik. A detailed description of a similar experimental setup at Ruhr-Universität Bochum can be found in Sengen et al. (2017). The service fluid was heated while flowing in a circular fashion, until a steady state temperature was reached. The temperatures measured by the four sensors were then recorded once per second for 60 s to calculate average temperatures. This was done for a range of service temperatures and process fluid flow rates, allowing some time between each adjustment to ensure a steady state temperature field. The measurement uncertainty is estimated to be between ±0.3 °C and ±0.5 °C. Selected experimental results are shown in Section 3 and provide the basis for the CFD simulations.

2.3. CFD setup

In the CFD simulations, we use the following assumptions: For the fluid dynamics simulations of the process fluid, we assume that the physical properties do not change with temperature, and instead use water properties at 30 °C. The steady-state three-dimensional flow field is computed first, and the heat transfer in a second step, using the results of the fluid simulation in a one-directional coupling. The same procedure is used for the service fluid (applicable in Level 3 only, see Section 2.4.3), except that we use water properties at 50 °C. The validity of this approach was confirmed with good accuracy with non-isothermal strongly-coupled simultaneous simulations, yielding similar results, but at a sharp increase in computational time. (The pressure loss and the temperatures computed with the nonisothermal approach were about 2 % and 0.25 °C, respectively, lower than when assuming constant fluid properties, at a cost of about 5 d and 16 h of additional runtime, even when initializing with the close solution obtained with the sequential approach. The resulting heat transfer coefficients were practically identical.) We conduct the simulations using the finite-element based software COMSOL Multiphysics (Anon) version 6.0, which is well-suited to multiphysics problems. We use the physics interface for single-phase laminar flow for the process fluid, since it is in the Reynolds number range of about 20 to 540, depending on the mass flow rate. For the service fluid, a mass flow rate of 10 kg/min corresponds to a maximum Reynolds number of about 19 000, so we use the turbulent k-ϵ model (again only applicable in Model refinement level 3). We further use the heat transfer in solids and fluids physics interfaces. Despite the small total volume of the millireactor, the complex geometry of its mixing elements and resulting process fluid domain requires a lot of detail and thus mesh elements to capture accurately. This is especially true on model refinement levels 2 and 3, where very thin gaps (0.075 mm) between the mixing elements have to be accounted for. Mesh convergence was verified for select cases to ensure that the obtained solutions are mesh-independent, but also do not use more mesh elements than necessary. Additionally, mesh skewness was used as a quality indicator, with all meshes having an average equiangular skew of less than 0.35. No error accumulation due to the small mesh element size, e.g., due to accumulation of numerical round-off errors, was observed. The simulations are run on a server with an Intel Xeon CPU with 8 physical and 16 logical cores with a clock rate of 2.4 GHz, and 192 GB RAM.

2.4. Levels of model refinement

To calculate the fluid flow and heat transfer inside the test channel, we set up a CFD model of the channel with three increasing levels of refinement. The idea is to start with a simple and computationally inexpensive model, and to then refine this model if necessary to achieve the desired accuracy.

2.4.1. Model refinement level 1

For the simplest model refinement level, we remove the small gaps between the mixing elements and channel walls by slightly upscaling the elements. This has the advantage that meshing the resulting geometry is much easier and requires far fewer elements, speeding up the computation. We also simplify the process fluid inlet and outlet sections by extending the channel by 2 mm on each end and omitting the inlet and outlet ports, as they have a negligible influence on the heat transfer. As stated above, we use a process fluid with constant material

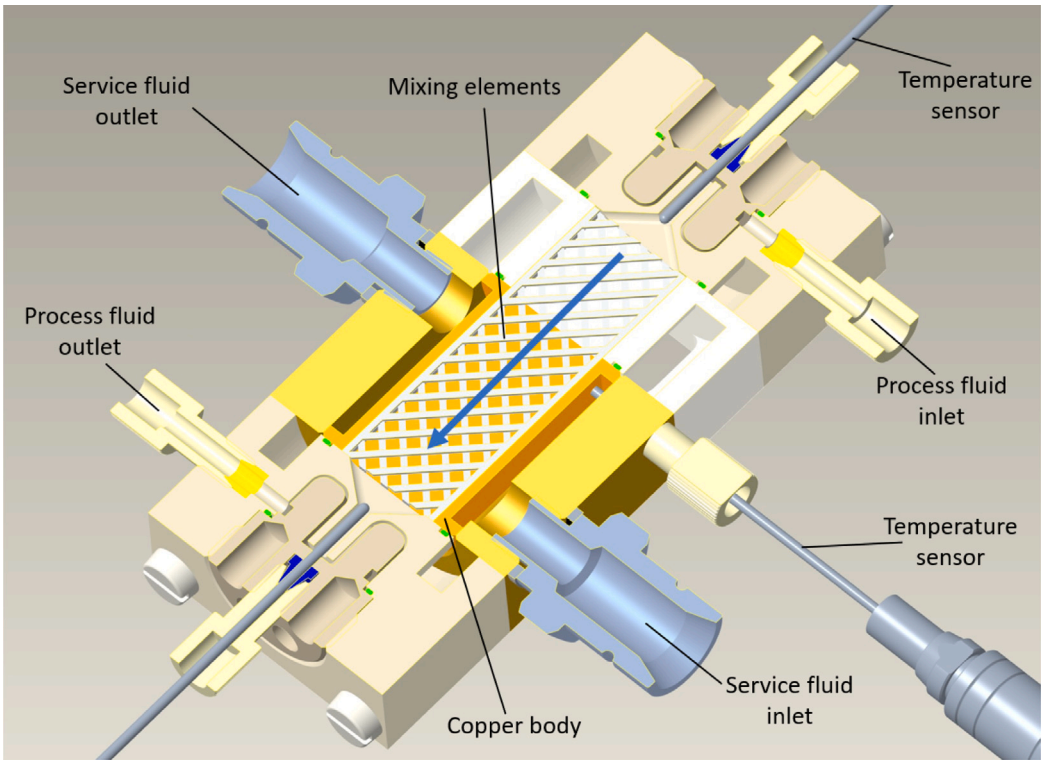

Fig. 1. A cutaway showing the lower half of the test channel. The main flow direction of the process fluid is indicated by the blue arrow.

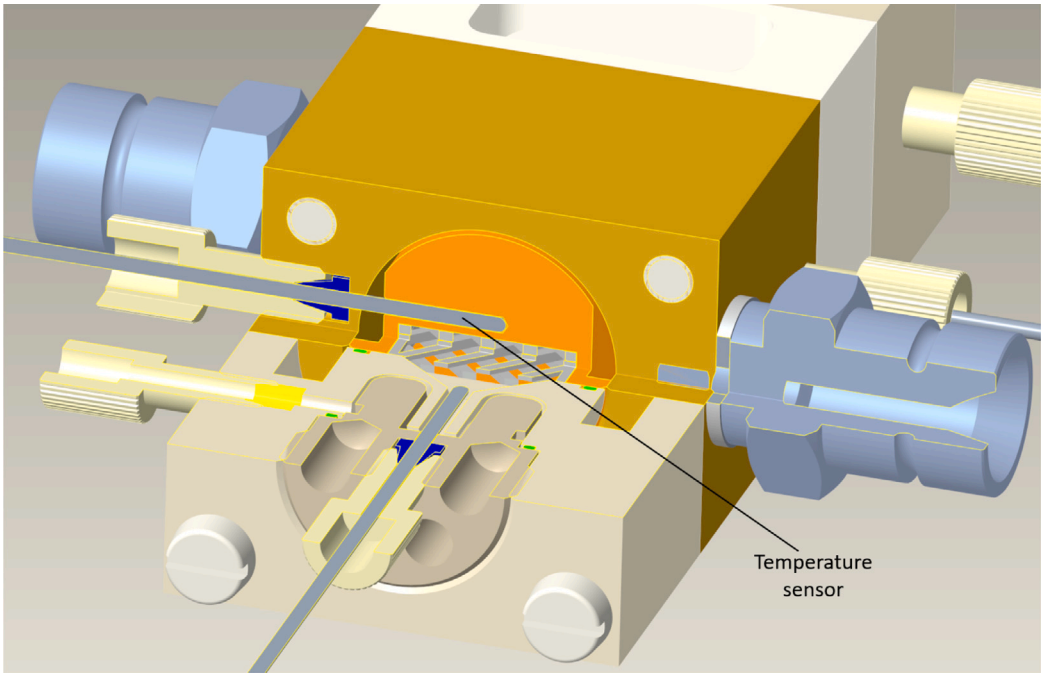

Fig. 2. A picture showing the position of the temperature sensor in the copper block near the channel outlet.

properties corresponding to water at 30 °C. For the steel, copper, brass, and PTFE parts of the channel, the relevant material properties are given in Table 1 and are assumed to be constant.

At this model refinement level, we assume that the service fluid flows sufficiently fast and therefore its temperature does not significantly change from inlet to outlet; thus, we do not explicitly model the service fluid but rather impose a fixed wall temperature of 50.5 °C on all surfaces which would otherwise be in contact with the service fluid. As the channel is symmetrical, we only model the lower half. Fig. 3 shows the different domains of the model and the heated wall. The mesh element size is between 0.05 mm to 0.15 mm. The resulting mesh for this model refinement level has about 9.1×10^6 elements, of which 2.9×10^6 elements account for the process fluid domain. Computing a steady state flow field takes between 6 h and 1.4 d (wall time), depending

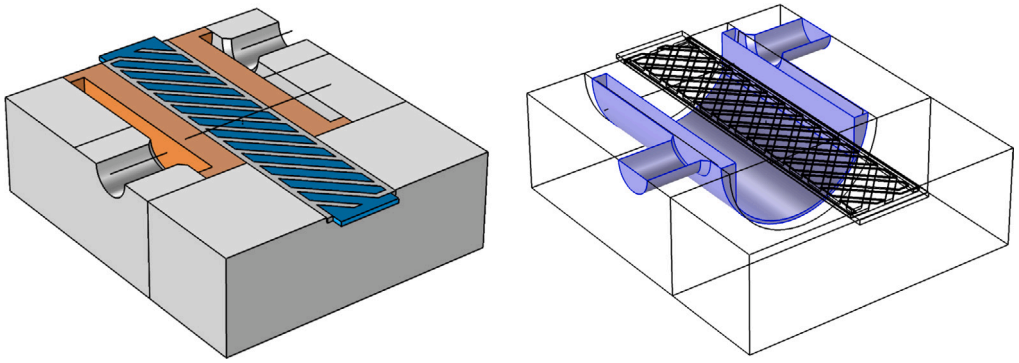

Fig. 3. On the left, the different domains of the Level 1 model are displayed, with the process fluid highlighted in blue and the copper heat transfer body in orange. On the right, the heated walls are highlighted in blue.

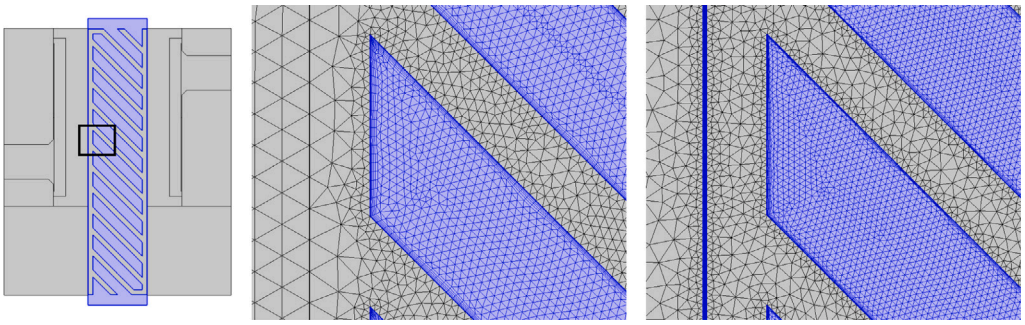

Fig. 4. Mesh comparison. On the left, the black rectangle highlights the position of the zoomed in area showing the level 1 (middle) and level 2 (right) meshes. On Level 1, the mixing elements and channel walls are in direct contact, while on Level 2 they are separated by a gap, visible as a thick blue vertical line. This line is comprised of mesh elements that are still too small to see in the selected zoom setting. It is however visible that these small elements also lead to a finer discretization of the connecting walls and mixing elements.

Table 1
Material properties of the test channel.

	ρ [kg/m^3]	Cp [J/(kg K)]	k [W/(m K)]
steel	7900	500	15
copper	8700	385	330
brass	8400	377	120
PTFE	2200	960	0.25

on the mass flow rate and initial conditions, and 18 GB of memory. Computing a temperature profile takes between 3 min and 17 min, again depending on the initial conditions.

2.4.2. Model refinement level 2

In contrast to the refinement level 1, the gaps between the individual mixing elements, as well as the elements and channel walls are included in the model refinement level 2. All other aspects are identical to Level 1. This necessitates a significantly finer mesh with a total of 20.4×10^6 elements and 11.1×10^6 elements for the process fluid domain. The size of the individual mesh elements is between 0.01 mm to 0.1 mm. Fig. 4 shows a comparison between the level 1 and 2 meshes. Computing a steady state flow field takes between 10 h and 3.5 d, using 87 GB to 120 GB of memory, depending on the mass flow rate and initial conditions. Computing a temperature profile takes about 1.5 h when initializing the entire domain with a fixed temperature, but as little as 10 min when using a close previous solution as the initial condition.

2.4.3. Model refinement level 3

For the third refinement level, the service fluid is also modeled, thus eliminating the simplification of using heated walls. For the service fluid, we assume constant material properties corresponding to water at 50 °C. The process fluid properties remain those of water at 30 °C. A flow rate of 10 kg/min and inlet temperature of 50.5 °C is used for the service fluid in accordance with the experiments. Including the service fluid domain adds about 4.8×10^6 mesh elements. All other aspects remain identical to Level 2. Computing an isothermal service fluid flow field takes about 12 h. The isothermal process fluid flow fields from refinement level 2 can be re-used, and computing a temperature profile does not take significantly longer than on refinement level 2.

Instead of directly combining the first improvement (adding the gaps between the mixing elements) and the second improvement (modeling the service fluid), it might be interesting to also explore the second improvement independently as an intermediary step. The reason we skip this step is that the pressure loss comparison between the Level 1 simulations and experiments (cf. Section 3.1) indicates that Level 1 cannot accurately capture the fluid flow of the process fluid. Since the fluid flow influences the heat transfer, we concentrate on further improving the more accurate Level 2.

2.5. Heat transfer coefficient

We are interested in the overall heat transfer coefficient α of the test channel. It is calculated in the following way:

$$\alpha_{\mathrm{PM}} = \frac{\dot{Q}_{\mathrm{PM}}}{A\ \Delta T_{\mathrm{ln,center}}} \tag{1}$$

$$\dot{Q}_{\mathrm{PM}} = \dot{m}\ c_{\mathrm{p,PM}}(T_{\mathrm{PM,out}} - T_{\mathrm{PM,in}}) \tag{2}$$

$$\Delta T_{\mathrm{ln,center}} = \frac{\Delta T_{\mathrm{out}} - \Delta T_{\mathrm{in}}}{\ln\left(\frac{\Delta T_{\mathrm{out}}}{\Delta T_{\mathrm{in}}}\right)} \tag{3}$$

$$\Delta T_{\mathrm{out}} = T_{\mathrm{W,out}} - T_{\mathrm{PM,out}} \tag{4}$$

$$\Delta T_{\mathrm{in}} = T_{\mathrm{W,in}} - T_{\mathrm{PM,in}} \tag{5}$$

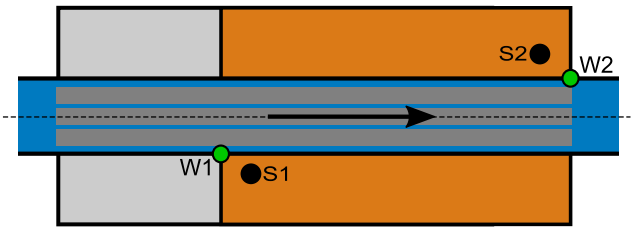

Fig. 5. Sideview schematic of the channel showing the temperature evaluation points (not to scale). The arrow indicates the main flow direction. The dark gray rectangles represent the mixing elements. The black dots denoted S1 and S2 represent the positions of temperature sensors 1 and 2, respectively. The green dots denoted W1 and W2 show the positions at the channel wall inlet and exit where we additionally extract temperatures from the simulations. Since by symmetry we do not include the upper half of the channel, the positions of points S2 and W2 are actually mirrored along the dashed line in our model.

The process fluid mass flow rate $\dot{m}$, thermal capacity $c_{p,PM}$, and inlet temperature $T_{PM,in}$ are model inputs. The area A is the area of the walls of the empty channel, equal to $(1.5\,\text{mm} + 12\,\text{mm}) \times 2 \times 36\,\text{mm} = 972\,\text{mm}^2$. The process fluid outlet temperature $T_{PM,out}$ and the wall temperatures at the beginning and end of the heat transfer part of the channel, $T_{W,in}$ and $T_{W,out}$, respectively, are calculated with the CFD model. As we described above, in the experiments, these are not really the temperatures right at the wall, but at the sensor positions, 2.45 mm away from the channel wall, and 3.5 mm away from the start and end of the heat transfer section of the channel. In the simulations, however, we are able to extract temperature information at arbitrary points inside the domain. We use these true (simulated) wall temperatures to compute corrected heat transfer coefficient values. The positions of the physical and virtual sensor points are shown in Fig. 5.

3. Results

3.1. Comparison of the model refinement levels

We now present the simulation results of the three model refinement levels and compare them with each other and with experiments, focusing first on refinement Levels 1 and 2. We begin by looking at the pressure loss over the channel. The pressure loss is a good indicator for the quality of the fluid dynamics simulations. Since the heat transfer simulations rely on velocity data, it is important to have an accurate process fluid flow field. Fig. 6 compares the pressure loss from channel inlet to outlet for different mass flow rates. The experimental pressure losses were measured with the full Miprowa Lab reactor with eight process channels with a total length of 2400 mm plus flow redirection sections between them, while the simulated losses were calculated using the test channel, and then extrapolated. Consequently, this is not a perfect comparison, but nevertheless serves to give a first estimate or impression of the performance of the model refinement levels 1 and 2. We see that the Level 1 simulations over-predict the pressure loss by over 50 % for mass flow rates of 200 g/min and over, while the results obtained with Level 2 provide a good match.

Next, we consider the temperatures at the sensor positions inside the copper block surrounding the channel (Points S1 and S2 in Fig. 5). The inlet temperature of the process fluid is about 26 °C, with small variations for each experimental evaluation. In the simulations, the exact inlet temperatures measured during each corresponding experiment are used. Recall that in the simulations on model refinement level 1 and 2, we assume a fixed wall temperature on the outside of the copper body surrounding the channel (cf. Fig. 3). Unfortunately, the inlet and exit temperatures of the service fluid were not recorded during this experimental series, but a temperature decrease of about 0.5 °C to 1.5 °C from inlet to outlet, depending on the flow rate of the process fluid, was observed in earlier experiments.

Fig. 7 shows the temperatures corresponding to the different refinement levels and mass flow rates. The temperatures at point S1 (i.e., the sensor position near the beginning of the channel) are slightly lower than those at point S2, because the process fluid is still cooler near the inlet. There is some qualitative agreement between the experiments and simulations, but an increasing mismatch with higher mass flow rates. Surprisingly, the temperatures obtained with model refinement level 1 are lower and closer to the experimental values than those of level 2.

Fig. 8 shows the outlet temperatures of the process fluid. Here, the results are reversed: While the slopes of the Level 1 and 2 curves are similar, the temperatures computed with Level 1 are about 3 °C higher

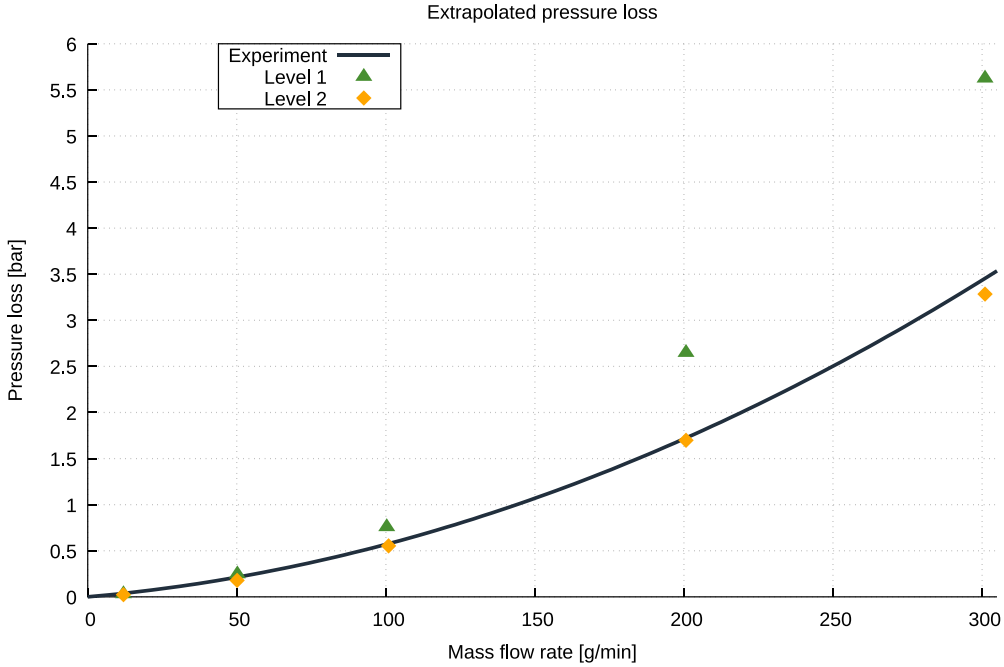

Fig. 6. An experimentally obtained pressure loss correlation is compared to the simulated pressure losses using different model refinement levels. On model refinement level 1, the gaps between the mixing elements and channel walls are neglected (cf. Section 2.4.1), resulting in an over-prediction of the pressure loss. On model refinement level 2, which includes the gaps, the simulation results are in close agreement with the experiments.

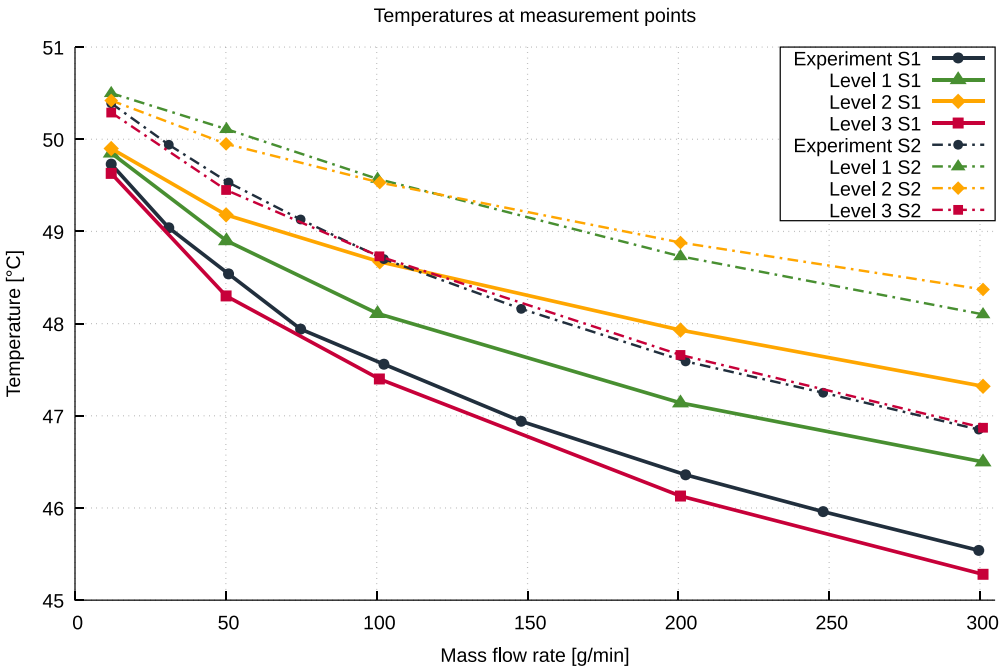

Fig. 7. Temperatures at the measurement points inside the copper body. The experimentally obtained values are compared to simulations using the three model refinement levels for different flow rates of the process fluid. The lines between the data points are interpolations and purely for visualization purposes. As the process fluid heats up as it passes through the channel, the temperatures at point S2 are higher than at point S1.

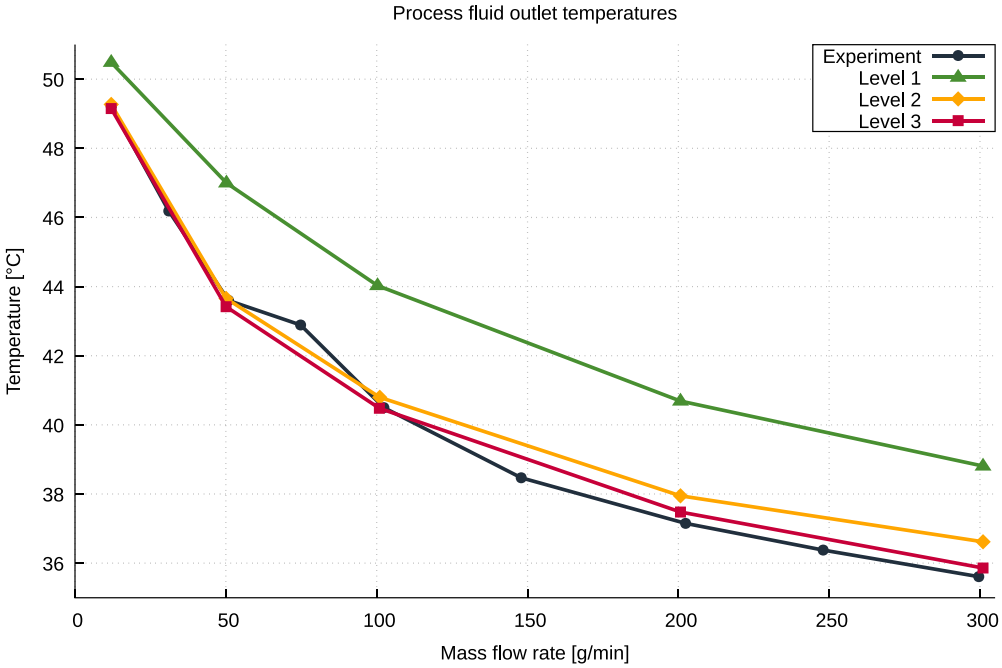

Fig. 8. Process fluid temperatures at the channel outlet. The simulated temperatures have been averaged over the outlet cross section.

than those of Level 2. Again, the difference increases with the wall temperature, which is expected.

Fig. 9 shows the temperatures on the symmetry plane through the middle of the channel. On Level 1, the mixing elements are in direct contact with the channel walls and each other, resulting in much hotter elements and consequently faster heating of the process fluid. On Level 2, the small gaps between the channel walls and elements keep the mixing elements cooler and keep hot spots from forming.

In Conclusion, it appears as though direct contact between the mixing elements and channel walls on Level 1 raises the effectiveness of the heat exchange between the process fluid and channel. The process fluid heats up faster, and in doing so transports away more energy, cooling the copper body more effectively than on Level 2. Even though this results in the observed lower temperatures inside the copper body (cf. Fig. 7), when looking at the outlet temperatures (cf. Fig. 8), the simplifications to get rid of the small gaps on modeling level 1 result in a model which deviates significantly from the experimental observations. When looking at Level 2, the increasing deviation from the experimental results with higher mass flow rates of the process fluid indicates that the process fluid in the experiments is not heated as

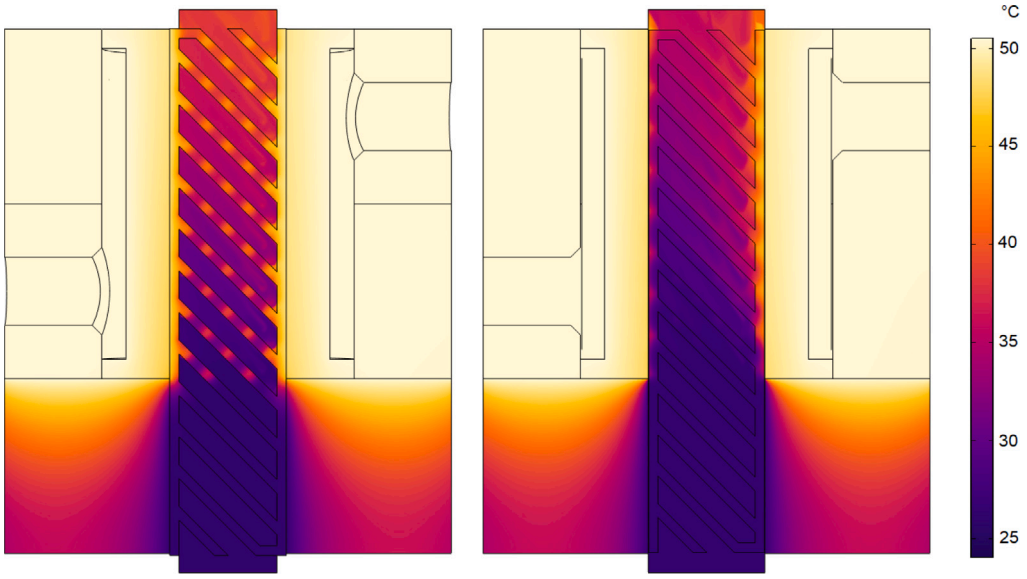

Fig. 9. Temperatures at the symmetry plane in the middle of the test channel. On the left, the mixing elements are in direct contact with the channel walls and each other (Level 1), while on the right, there are small gaps between the elements and the walls (Level 2). The direct contact results in much hotter elements, which leads to faster heating of the process fluid. The hot spots on the visible central mixing element are caused by contact with the mixing element below, which is itself in contact with the hot wall.

effectively as in the simulations, raising the question if the assumption of a fixed wall temperature on the service side is too strong.

We now compare the results obtained by using the model refinement level 2 to those obtained with level 3, and again compare both to experimental measurements. Recall that on model refinement level 3, the heating of the process fluid is no longer achieved by setting a wall temperature on the outside of the copper body, but by including the service fluid in the model. The process fluid again has an inlet temperature of about 26 °C, with variations of up to 0.5 °C that were matched in the simulations.

Referring again to Fig. 7, we see a considerable difference between model refinement levels 2 and 3: While the temperatures obtained with Level 2 are consistently too high, and the gap between the simulations and experimental results increases with the mass flow rate of the process fluid, Level 3 matches with the experiments very well. There is almost perfect agreement between the measured and simulated temperatures at measurement point S2, and at measurement point S1, the simulated temperatures are slightly too low, but still close to the experimental values.

This leads to the conclusion that the assumption of a fixed wall temperature on the service side of the copper body is too strong. It appears that a service fluid mass flow rate of 10 kg/min is not quite sufficient to achieve a quasi-isothermal temperature distribution in the service fluid, but instead results in a small but non-negligible temperature drop along the flow path of the service fluid. As stated above, the nominal service fluid inlet temperature is 50.5 °C. In the Level 3 simulations, this temperature decreases by about 0.03 °C for a process fluid mass flow rate of 12 g/min, and 0.24 °C for 300 g/min. More importantly, the outer wall temperature of the copper body does not quite attain the temperature of the service fluid, but remains a few degrees Celsius colder. Fig. 10 shows the temperatures of the test channel, as well as the process and service fluids, on a cutplane through the channel for the case with a process fluid mass flow rate of 300 g/min.

Fig. 8 once more shows the average outlet temperatures of the process fluid. Here, the difference between the Level 2 and 3 results is not as pronounced as that observed for the measurement points, but particularly for higher mass flow rates of the process fluid, Level 3 clearly is a better match to the experimental measurements.

In conclusion, Level 3 yields a significantly better approximation of the experiments, at the cost of an also significantly more complex model.

3.2. Influence of the thermal conductivity

In this section, we examine the effect of a different thermal conductivity of the copper body. We increase the thermal conductivity of the copper body from 330 W/(m K) to 385 W/(m K). The motivation for this is that there is some uncertainty regarding the exact copper variant that was used in making this part of the test channel, and hence its thermal conductivity. When initially setting up the model, the previously used value of 330 W/(m K) was therefore used as an assumption. A later investigation showed however, that the copper body was likely made from copper type CW021 A, which has a thermal conductivity of 385 W/(m K).

We compare the results of the experiments and Level 3 simulations from the previous section with new Level 3 simulations using the higher thermal conductivity in Figs. 11 and 12. The first figure displays once more the temperatures at the measurement points. The simulated temperatures at measurement point S1, which are slightly to low when using a thermal conductivity of 330 W/(m K), match the experiments better with the higher conductivity. The situation is reversed at the second measurement point. The higher conductivity now leads to temperatures that are slightly too high, whereas they match perfectly in the case of lower conductivity. In both cases, the simulated temperature increase between the points S1 and S2 is a bit larger than the measured increase. Overall, both cases approximate the measurements equally well.

Fig. 12 shows the outlet temperatures of the process fluid. Up to a process fluid mass flow rate of 100 g/min, the difference between the cases is negligible. For a flow rate of 200 g/min and up, the higher thermal conductivity of the copper body leads to a slightly increased deviation from the measurements, compared to the “default” Level 3 simulation.

3.3. Obtaining the heat transfer coefficients

In the previous sections, we have demonstrated that simulations can closely approximate the heat transfer in the Miprowa test channel. A validated model can further be used instead of experiments to conduct additional test series, e.g., with a different wall temperature, or to extract additional information that is not experimentally accessible.

As we described earlier, the experimental setup does not allow to capture the true wall temperatures, but instead temperatures are

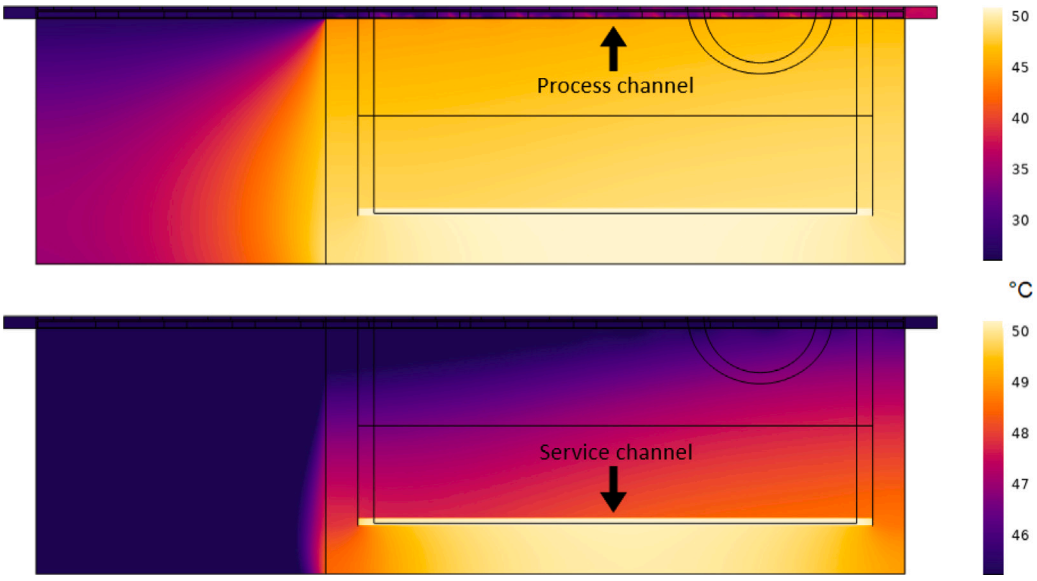

Fig. 10. A cut through the test channel. Both pictures show the same cutplane, but with differently scaled temperature ranges. The top picture shows the whole temperature range, highlighting the rising temperature of the process fluid as it flows though the channel (main flow direction from left to right). The bottom picture shows the temperature range of 45.5 °C to 50.5 °C, with anything colder than 45.5 °C appearing as dark blue. Here, the focus is on the service fluid, which is represented by the narrow white band. The copper body directly above the service fluid is a few degrees Celsius cooler than the service fluid itself, and warmer towards the end of the process channel (on the right) than near the inlet. Note that the main flow direction of the service fluid is perpendicular to, and into, the cutplane.

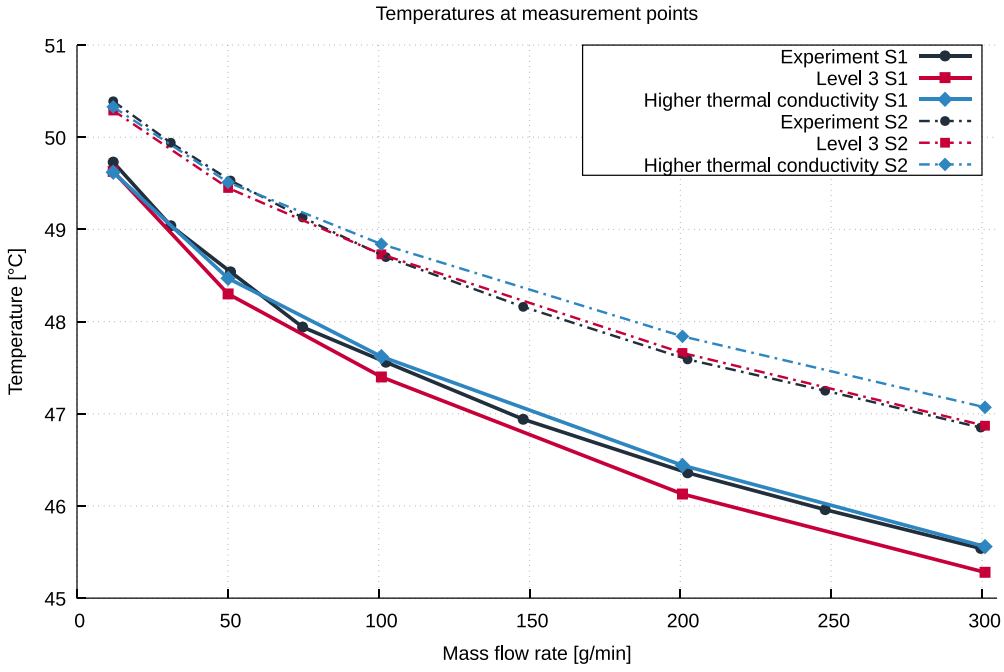

Fig. 11. Raising the thermal conductivity of the copper body also raises the simulated temperatures at both measurement points. This leads to a better match with the experimental values at point S1, but to a worse fit at point S2.

measured at a small distance away from the wall. In the simulations, however, we are not constrained in this way and can evaluate the temperatures at any location in the computational domain. Thus, we can recover the missing wall temperatures from the validated simulation results. Refer again to Fig. 5 for the positions of the evaluation points. Fig. 13 shows the temperatures at these points for the unmodified Level 3 simulations.

The temperatures at the wall (W1 & W2) are lower than at the corresponding sensor points in the copper block (S1 & S2), as should be expected due to the direct contact with the cool process fluid. Particularly interesting is the situation for low mass flow rates. In the hypothetical case of no flow of the process medium, all points would take on the service fluid inlet temperature, i.e., 50.5 °C. Nevertheless, even a low mass flow rate of 12 g/min is sufficient to induce a temperature difference of 0.6 °C between the measurement point in the copper body (S1) and the wall (W1) at the beginning of the heat transfer portion of the test channel. At the end of the channel (S2 & W2), where the process fluid has had time to heat up, the temperatures at and near the wall are almost identical. As we have seen before, the temperature differences again increase with the mass flow rate.

Since we have just seen that the temperatures at the wall are significantly lower than those measured merely near the wall, the

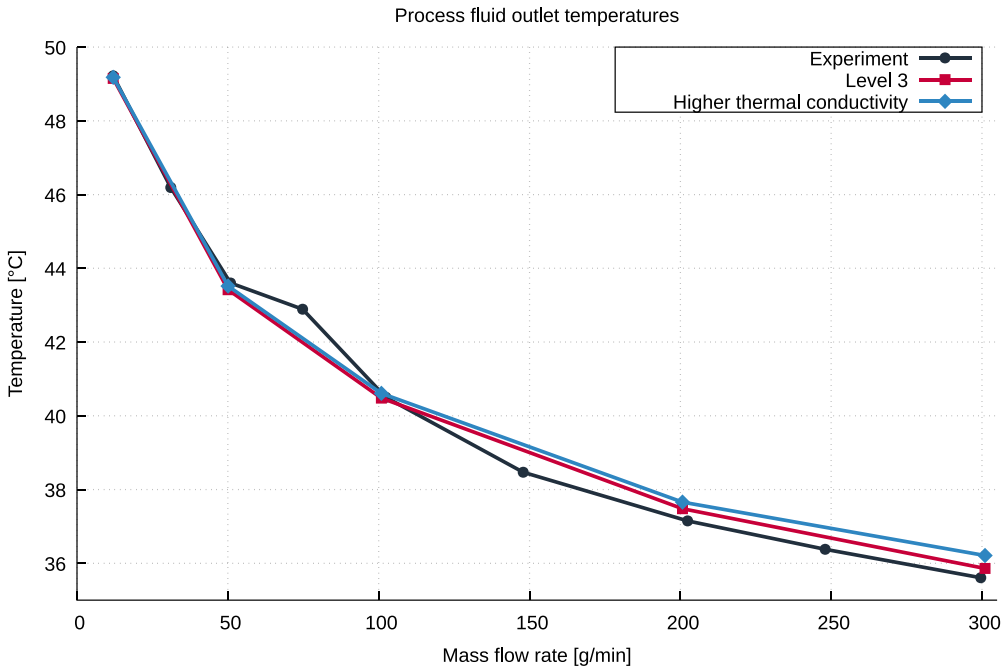

Fig. 12. The outlet temperatures in the unmodified Level 3 simulations are closer to the experimental values. Raising the thermal conductivity leads to an increasing over-prediction for higher mass flow rates.

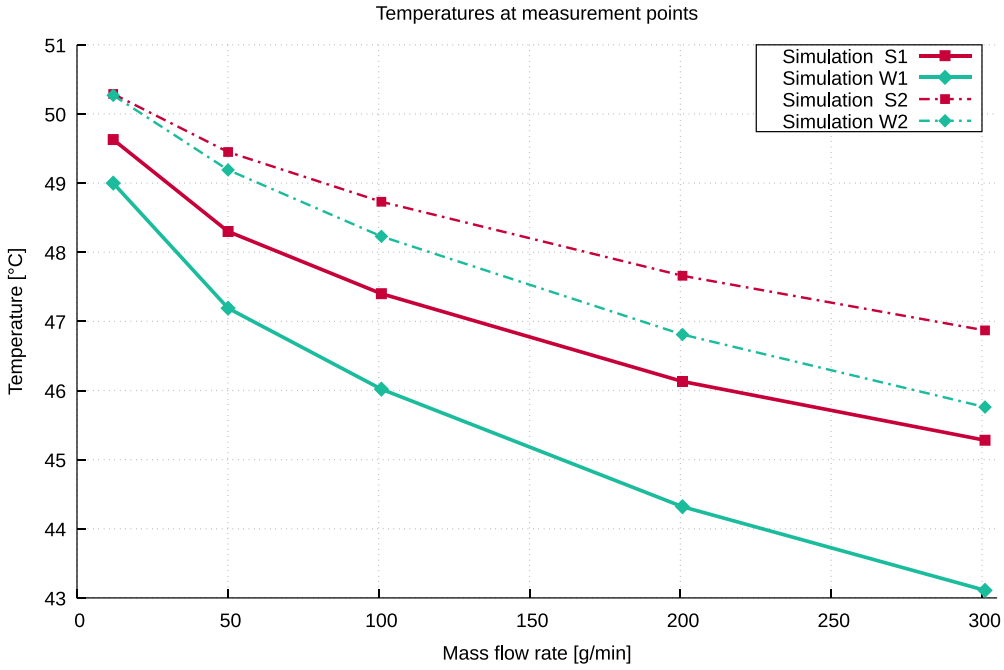

Fig. 13. Temperatures in the copper body surrounding the test channel (S1 & S2) and at the corresponding wall positions at the beginning and end of the heat transfer section of the channel (W1 & W2, respectively).

logical conclusion is to use these wall temperatures to calculate the heat transfer coefficients for the channel. This is what we have been interested in from the beginning, but could only approximate before. Using the equations presented in Section 2.5, the results are plotted in Fig. 14. The heat transfer coefficients calculated using the wall temperatures are up to 11 % higher than those using the simulated sensor temperatures. The deviation is increasing with the mass flow rate of the process fluid. This information can be used to make estimates about the real heat transfer coefficients of the channel and Miprowa reactor, and to correct the experimentally obtained values.

4. Conclusions

Continuous flow millireactors are important devices in the chemical industry. Due to their high complexity, characterizing them experimentally can be challenging, as not all relevant process data is easily accessible. In this case, we were interested in the heat transfer coefficients of the Miprowa Lab millireactor. Because of manufacturing limitations, evaluating the necessary temperatures at the reactor channel wall was not possible, and only approximate near-wall values could be measured. CFD simulations can help to gain a more complete

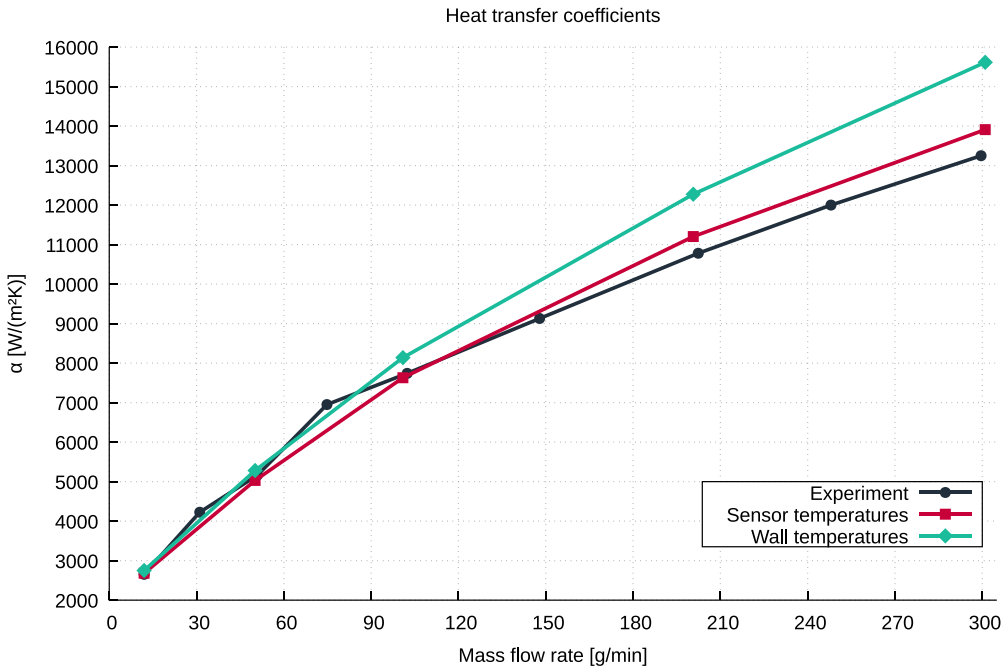

Fig. 14. The heat transfer coefficients of the test channel, computed using the experimentally obtained temperatures at the measurement points, the simulated temperatures at these same points, and the simulated wall temperatures. Using the wall temperatures results in a heat transfer coefficient that is up to 11 % higher than using the (simulated) near-wall temperatures for a given mass flow rate.

understanding by offering a "look inside" the system or process under examination, and by making additional information available. We have shown that our simulation model can replicate the experiments with varying degrees of accuracy, depending on the selected refinement level, and that particularly the most detailed model agrees with the experiments well. We have then used this model to compute the previously unknown wall temperatures, and used these to calculate the heat transfer coefficients. The obtained coefficients were up to 11 % higher than when using the temperatures at the sensor positions, showing that relying on experiments alone would have resulted in a significant underestimation of this important characteristic. Future work could attempt to further improve the model, and to use it to study e.g. the influence of different mixing element geometries, or of process fluids with different viscosities and thermal conductivities, on the heat transfer.

CRediT authorship contribution statement

Moritz J. Begall: Conceptualization, Investigation, Methodology, Validation, Visualization, Writing – original draft. **Frank Herbstritt:** Conceptualization, Investigation, Writing – review & editing. **Anne-Laura Sengen:** Investigation. **Adel Mhamdi:** Funding acquisition, Project administration, Writing – review & editing. **Joachim Heck:** Resources. **Alexander Mitsos:** Funding acquisition, Resources, Supervision, Writing – review & editing.

Declaration of competing interest

The RWTH authors have no conflict of interest. The Ehrfeld authors have commercial interest in the reactor but to our best of knowledge this does not affect the simulations or experiments.

Data availability

All data generated or analyzed during this study is included in the article and its supplementary information file.

Acknowledgments

The work presented in this article was conducted as a part of the KoPPonA project, a research project concerned with the development of an efficient overall concept for continuously operated processes for specialty polymer production. The support of the German Federal Ministry for Economic Affairs and Energy (BMWi) under grant number 03ET1183C is gratefully acknowledged. For more information, see http://enpro-initiative.de/en/KoPPonA.html.

Appendix A. Supplementary data

Supplementary material related to this article can be found online at https://doi.org/10.1016/j.compchemeng.2024.108621.

References

Amini, E., Mehrnia, M.R., Mousavi, S.M., Mostoufi, N., 2013. Experimental study and computational fluid dynamics simulation of a full-scale membrane bioreactor for municipal wastewater treatment application. Ind. Eng. Chem. Res. 52 (29), 9930–9939. http://dx.doi.org/10.1021/ie400632y.

An, H., Li, A., Sasmito, A.P., Kurnia, J.C., Jangam, S.V., Mujumdar, A.S., 2012. Computational Fluid Dynamics (CFD) analysis of micro-reactor performance: Effect of various configurations. Chem. Eng. Sci. 75, 85–95. http://dx.doi.org/10.1016/j.ces.2012.03.004, URL http://www.sciencedirect.com/science/article/pii/S0009250912001674.

Anon, 2021. COMSOL Multiphysics v. 6.0 release website, COMSOL AB, Stockholm, Sweden, URL https://www.comsol.com/release/6.0.

Begall, M.J., Krieger, A., Recker, S., Herbstritt, F., Mhamdi, A., Mitsos, A., 2018. Reducing the fouling potential in a continuous polymerization millireactor via geometry modification. Ind. Eng. Chem. Res. 57 (18), 6080–6087. http://dx.doi.org/10.1021/acs.iecr.8b00206.

Begall, M.J., Schweidtmann, A.M., Mhamdi, A., Mitsos, A., 2023. Geometry optimization of a continuous millireactor via CFD and Bayesian optimization. Comput. Chem. Eng. 171, 108140. http://dx.doi.org/10.1016/j.compchemeng.2023.108140, URL https://www.sciencedirect.com/science/article/pii/S0098135423000091.

Brahim, F., Augustin, W., Bohnet, M., 2003. Numerical simulation of the fouling process. Int. J. Therm. Sci. 42 (3), 323–334. http://dx.doi.org/10.1016/S1290-0729(02)00021-2, URL http://www.sciencedirect.com/science/article/pii/S1290072902000212.

Buchelli, A., Call, M.L., Brown, A.L., Bird, A., Hearn, S., Hannon, J., 2005. Modeling fouling effects in LDPE tubular polymerization reactors. 2. Heat transfer, computational fluid dynamics, and phase equilibria. Ind. Eng. Chem. Res. 44 (5), 1480–1492. http://dx.doi.org/10.1021/ie040158i.

Calabrese, G.S., Pissavini, S., 2011. From batch to continuous flow processing in chemicals manufacturing. AIChE J. 57 (4), 828–834. http://dx.doi.org/10.1002/aic.12598.

Gao, X., Shi, D.-P., Chen, X.-Z., Luo, Z.-H., 2010. Three-dimensional CFD model of the temperature field for a pilot-plant tubular loop polymerization reactor. Powder Technol. 203 (3), 574–590. http://dx.doi.org/10.1016/j.powtec.2010.06.025, URL https://www.sciencedirect.com/science/article/pii/S0032591010003244.

Gobert, S.R.L., Kuhn, S., Braeken, L., Thomassen, L.C.J., 2017. Characterization of milli- and microflow reactors: Mixing efficiency and residence time distribution. Org. Process Res. Dev. 21 (4), 531–542. http://dx.doi.org/10.1021/acs.oprd.6b00359.

Gürsel, I.V., Hessel, V., Wang, Q., Noël, T., Lang, J., 2012. Window of opportunity – Potential of increase in profitability using modular compact plants and microreactor based flow processing. Green Process. Synth. 1, 315–336. http://dx.doi.org/10.1515/gps-2012-0046, URL www.degruyter.com/view/j/gps.2012.1.issue-4/gps-2012-0046/gps-2012-0046.xml.

Jensen, K.F., 2017. Flow chemistry—Microreaction technology comes of age. AIChE J. 63 (3), 858–869. http://dx.doi.org/10.1002/aic.15642.

Mitsos, A., Chachuat, B., Barton, P.I., 2007. Methodology for the design of man-portable power generation devices. Ind. Eng. Chem. Res. 46 (22), 7164–7176. http://dx.doi.org/10.1021/ie070586z.

Mitsos, A., Palou-Rivera, I., Barton, P.I., 2004. Alternatives for micropower generation processes. Ind. Eng. Chem. Res. 43 (1), 74–84. http://dx.doi.org/10.1021/ie0304917.

Rahimi, M., Madaeni, S., Abolhasani, M., Alsairafi, A.A., 2009. CFD and experimental studies of fouling of a microfiltration membrane. Chem. Eng. Process. 48 (9), 1405–1413. http://dx.doi.org/10.1016/j.cep.2009.07.008, URL http://www.sciencedirect.com/science/article/pii/S025527010900124X.

Roberge, D., Noti, C., Irle, E., Eyholzer, M., Rittiner, B., Penn, G., Sedelmeier, G., Schenkel, B., 2014. Control of hazardous processes in flow: Synthesis of 2-nitroethanol. J. Flow Chem. 4 (1), 26–34. http://dx.doi.org/10.1556/JFC-D-13-00016.

Rodríguez-Guerra, Y., Gerling, L.A., López-Guajardo, E.A., Lozano-García, F.J., Nigam, K.D.P., Montesinos-Castellanos, A., 2016. Design of micro- and milli-channel heat exchanger reactors for homogeneous exothermic reactions in the laminar regime. Ind. Eng. Chem. Res. 55 (22), 6435–6442. http://dx.doi.org/10.1021/acs.iecr.6b00323.

Schönfeld, F., Hardt, S., 2004. Simulation of helical flows in microchannels. AIChE J. 50 (4), 771–778. http://dx.doi.org/10.1002/aic.10071.

Sengen, A.-L., Herbstritt, F., Grünewald, M., Heck, J., 2017. Experimentelle Bestimmung des konvektiven Wärmeübergangs in einem mikrostrukturierten Kanal. Chem. Ing. Tech. 89 (4), 379–389. http://dx.doi.org/10.1002/cite.201600163.

Shi, X., Xiang, Y., Wen, L.-X., Chen, J.-F., 2012. CFD analysis of flow patterns and micromixing efficiency in a Y-type microchannel reactor. Ind. Eng. Chem. Res. 51 (43), 13944–13952. http://dx.doi.org/10.1021/ie300985q.

Woldemariam, M., Filimonov, R., Purtonen, T., Sorvari, J., Koiranen, T., Eskelinen, H., 2016. Mixing performance evaluation of additive manufactured milli-scale reactors. Chem. Eng. Sci. 152, 26–34. http://dx.doi.org/10.1016/j.ces.2016.05.030, URL http://www.sciencedirect.com/science/article/pii/S0009250916302780.